Electrical Power and Energy Systems 130 (2021) 106933

Contents lists available at ScienceDirect

International Journal of Electrical Power and Energy Systems

journal homepage: www.elsevier.com/locate/ijepes

Interpretation of transformer winding deformation fault by the spectral clustering of FRA signature

Zhongyong Zhao [a,*], Chao Tang [a], Yu Chen [a], Qu Zhou [a], Chenguo Yao [b], Syed Islam [c]

[a] College of Engineering and Technology, Southwest University, Chongqing 400716, China
[b] State Key Laboratory of Power Transmission Equipment & System Security and New Technology, School of Electrical Engineering, Chongqing University, Chongqing 400044, China
[c] School of Science Engineering and Information Technology, Federation University, Melbourne, Australia

ARTICLE INFO

Keywords:
Fault analysis
Power transformers
Artificial intelligence
Spectral clustering
Winding deformation

ABSTRACT

Frequency response analysis (FRA) has been accepted as a widely used tool for the power industry. The interpretation of FRA can be achieved by the conventional mathematical indicators-based method, which is mostly used in the past. The newly developing artificial intelligence (AI)-based method also provides an alternative interpretation. However, in most reported AI techniques, the features of FRA signatures are directly input into the AI model to obtain the classification results. Few studies have concentrated on the separability of winding deformation faults. In this context, a spectral clustering algorithm is studied to aid in FRA interpretation. The electrical model simulation and experimental tests are performed. The FRA data processing results verify the feasibility, effectiveness and superiority of the proposed method.

1. Introduction

As the heart of a substation, the power transformer functions as the significant link of voltage conversion and energy delivery [1]. When transformers are out of service due to significant faults, electricity asset holders will lose millions of dollars; furthermore, a substantial amount of manpower and financial resources are required for transformer maintenance, which further reduce their economic benefits. Transformer faults are divided into external and internal faults [2]. Among internal faults, the active part mechanical faults of a transformer are more significant [3]. These faults include winding displacement or deformation, bending, tilting, bucking, spiraling, transformer core faults and faults related the load tap changer [4]. Among them, winding deformation fault do great harm to the normal operation of transformer, and it is of significance to detect and diagnose it in the early stage.

Recently, a variety of winding deformation fault detection methods has been successively proposed. The main methods include the vibration method [5], the ultra-wideband (UWB) antenna method [6], short circuit impedance (SCI) [7], low voltage impulse (LVI) [8], the voltage-current Locus diagram [9] and the frequency response analysis (FRA) method [10]. Some of these approaches are offline methods, which are successfully adopted in the field [7,8,10], while some online methods are still in the developmental stage [5,6,9]. Among the above methods, FRA has proven to be a reliable, simple, fast, economic and non-destructive diagnostic tool [10], which is widely accepted. In FRA, the transformer frequency response signatures with frequency bands of 20 Hz ~ 2 MHz are often used for analysis, and information about the winding mechanical structure can be observed in this wide frequency band. At present, FRA has already been commercialized. Chinese power industry standards [11] and IEC standards [12] have been successively proposed to standardize the technique.

FRA is considered to be a comparative method. Time-based comparison, construction-based comparison and type-based comparison methods have been developed. The measured FRA signature is compared with its "fingerprint", sometimes the data of the other phases or the data of the sister unit, to analyze potential failures. The "fingerprint" is the measured FRA signature when the transformer has a healthy status. Besides, the time-based comparison method is more reliable. Currently, the accurate interpretation of FRA data still remains a challenge. The current FRA interpretation technique mostly depends on visual inspection [13]. The FRA signatures are divided into low-frequency, mid-frequency and high-frequency bands, and the observations are performed over each frequency band. This technique calls for experienced personnel and prior knowledge about the impact of transformer variable winding faults on each frequency range, which is likely to cause false positives and false negatives. To obtain a more reliable FRA

* Corresponding author.

https://doi.org/10.1016/j.ijepes.2021.106933
Received 9 June 2020; Received in revised form 15 January 2021; Accepted 19 February 2021
Available online 21 March 2021

interpretation code, considerable research efforts have been carried out, and these works can be divided into two categories:

1) Conventional FRA interpretation method

The main interpretation code is mainly based on mathematical statistical indicators. Since the last decade when FRA was introduced, many statistical indicators have been proposed, including the correlation coefficient (CC), the absolute sum of logarithmic error (ASLE), and the standard deviation (SD), etc. The statistical indicators are computed and extracted from two FRA traces to evaluate the winding faults by comparing the indicator value with the threshold value. For instance, the relative factors of two FRA traces of 1–100 kHz, 100–600 kHz and 600–1000 kHz are recommended in the Chinese standard DL/T 911 [11]. E. Rahimpour comprehensively compared frequency and amplitude deviation, standardized difference area, weight function and other indexes to evaluate winding radial, axial and inter-turn faults [14]. IEC 60076-18 and IEEE C57.149-2012 also recommend the use of some other indicators [12]. The recently used statistical indicators were summarized by Samimi [15–16]. Besides, there is an FRA interpretation method based on transformer electric circuits [17–18]. However, the statistical indicator method has room for improvement; moreover, the method based on the electric circuit calls for modeling the winding at the initial stage, which is always a complexity.

2) Advanced artificial intelligent FRA interpretation method

Some researchers have turned to artificial intelligence (AI) [19]. M. Bigdeli applied a support vector machine (SVM) algorithm to classify winding faults, in which the frequency-amplitude and the poles of transfer function (TF) were used [20]. Furthermore, [21] improved the classifying performance by combining a genetic algorithm (GA) and a particle swarm optimization (PSO) algorithm with an SVM, and this method was successfully verified on an actual model transformer. In addition, artificial neural networks (ANN) have also been applied for transformer winding fault detection. In [22], a novel intelligent diagnosis method was proposed to diagnose winding inter-disk fault, in which all the frequencies of the FRA trace are used for model construction.

In most of above AI techniques, the features of FRA signatures are directly input into the AI model, and the classification results of winding faults are obtained. The authors suggest that few studies have concentrated on the separability of winding deformation faults. In this context, the purpose of this study is not to train an AI model for fault classification from the perspective of supervised learning; instead, the clustering analysis is applied to aid in FRA interpretation. However, conventional clustering techniques, such as *K*-means, are more suitable for convex sets, while the dimensions of FRA features can be high, and the distribution of these feature sets may not be convex. Hence, another AI algorithm spectral clustering is introduced in this paper, and it is not sensitive to the distribution shape of a dataset, and can solve very general problems like intertwined spirals [23].

2. Theoretical analysis

2.1. Mathematical principle of spectral clustering algorithm

From the perspective of graph theory, spectral clustering can be regarded as a graph segmentation problem. Given a graph $G = (V, E)$, vertex set V represents the samples, and the weighted edge E represents the similarity between the samples. The aim of spectral clustering is to find a reasonable method for dividing graphs [24–25].

Let $A_1, \cdots, A_k$ be the subsets of a graph. To minimize the cut value of segmentation, the spectral clustering minimizes the original objective function [20],

$$cut(A_1, \cdots, A_k) = \frac{1}{2}\sum_{i=1}^{k} W(A_i, \overline{A_i}) \tag{1}$$

where k is the number of groups into which the samples are divided, A_i is the ith group, $\overline{A_i}$ is the complementary set of A_i, and $W(A_i, \overline{A_i})$ is the sum of the weights of all edges between group $A_i$and $\overline{A_i}$.

The objective function of the spectral clustering algorithm is closely related to the Laplace matrix [23–24]. The divide criteria of different spectral clustering algorithms are diverse, and among the criterion, NJW (Ng-Jordan-Weiss) is the classical spectral clustering algorithm, which can be divided into the following steps:

1) Construct a similarity matrix

In spectral clustering, each sample point can be regarded as the vertex set of an undirected graph. The similarity of sample points is the edge of the undirected graph. The similarity matrix W is constructed by the weight of the edges, in which, W can be constructed through the methods of full connection, nearest neighbor, etc. [23]. The common Gauss kernel function is used to construct W in this study, as shown in Equation (2),

$$W_{i,j} = exp(-\frac{||x_i - x_j||^2}{2\sigma^2}) \tag{2}$$

where x_i and x_j are two sample points, σ is the parameter of the Gauss function, and $||||$ is the Euclidean paradigm.

2) Construct a Laplace matrix

The Degree matrix D is computed based on similarity matrix W. Further, the Laplace matrix is then constructed based on the degree matrix D. There exist three common methods: 1) construct the non-normalized Laplace matrix L of the undirected graph; 2) construct the normalized Laplace matrix L_{rm}, which is closely related to the random walk theory; 3) construct the normalized Laplace matrix L_{sym}. The third method, which is most commonly used, is adopted in this study, as shown in Eq. (3),

$$L_{sym} = D^{\frac{1}{2}} W D^{\frac{1}{2}} \tag{3}$$

where D is the degree matrix of an undirectional graph.

3) Clustering analysis

Compute the set of eigenvectors corresponding to the first k eigenvalues of L_{sym}, and construct feature vector space S of the sample data,

$$S = [v_1, v_2, \ldots v_k] \tag{4}$$

where $v_1, v_2, \ldots v_k$ are the k eigenvectors, corresponding to the first k eigenvalues in descending order.

Finally, the data points of feature vector space S are clustered by the *K*-means method, and the clustering result is mapped to the original sample space.

2.2. Analysis procedure based on the clustering algorithm

The FRA analysis procedure based on the spectral clustering

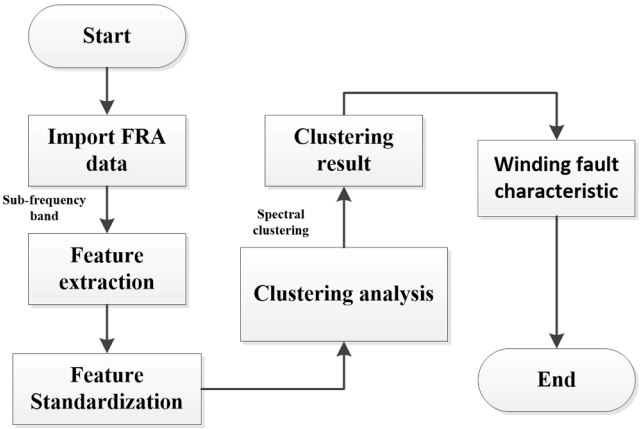

Fig. 1. Analysis procedure based on clustering analysis.

algorithm is shown in Fig. 1. The numbers of original FRA data with variable fault types, locations and degrees are collected, including simulation and experimental data. Due to FRA is a comparative method, some statistical indices can be calculated from FRA and its fingerprint to characterize the information of corresponding winding fault. These statistical indices, as the FRA statistical features, can be then input to the AI algorithm. In this study, several FRA statistical features are calculated within three sub-frequency bands, namely, 1–100 kHz, 100–600 kHz and 600–1000 kHz. More details about these features are introduced in Section III. Besides, to eliminate the influence of dimensions presented by different statistical features, a pre-processing is applied for feature standardization to obtain the samples. Then, the samples are processed by the spectral clustering algorithms. Finally, the clustering result is obtained, and the characteristic of FRA that winding deformation fault presents are analyzed.

3. Calculation of the fra statistical features and pre-processing

3.1. Calculation of the FRA statistical features

At present, many mathematical statistical indicators are calculated based on the measured FRA signatures and fingerprint [16]. The common statistical indicators can be divided into two categories: indicators based on the frequency and amplitude of the resonant points in the FRA signature and indicators based on all the data points of the FRA signature [26–27]. The accurate extraction of the resonant frequency and amplitude is required when the first indicators are calculated, and thus, these indicators are more easily influenced by the noise of FRA and the extraction algorithm [13]. The second indicators are simple, easily calculated, and less affected by noise. In this study, the second statistical indicators are calculated within the three sub-frequency bands to extract statistical features. The selected indicators include the Euclidean distance, sum squared ratio error, spectrum deviation, absolute sum of logarithmic error, correlation coefficient, normalized correlation coefficient, absolute difference, expectation, minimum–maximum ratio and standard deviation [1,10–11,13–14,22]. The abbreviation and calculation methods of these indicators can be found in Table 1.

3.2. Pre-processing of the statistical features

Different statistical features have different dimensions and units, which will have a significant impact on the results of clustering analysis if these features are directly input to the clustering algorithm. The input statistical features are pre-processed by a standardization method to eliminate the effect of dimensions.

The different fault types of transformer winding deformation will have significant impact on the different frequency bands of the FRA signature. Moreover, the FRA signature is mostly analyzed in the low-, mid-, and high- frequency band, respectively. Therefore, the FRA statistical feature dataset cannot be simply normalized by columns or rows because for a certain statistical indicator, this scheme will change the relative relation between the indicator values of different sub-frequency bands and cannot reflect the implied information of an FRA signature.

In this study, continuous three columns of dataset, namely a specific statistical indicator, are normalized. As shown in Table 2, indicators *ED* and CC are taken as examples for the feature construction. *L* indicates low frequency band, *M* indicates middle frequency band, *H* indicates high frequency band, and *No.* indicates the number of sample. If a statistical indicator is definitely smaller than 1, the value of this indicator in each sub-frequency band remains unchanged, for instance, the indicators *CC* and *MM*; if a statistical indicator is probably>1, this statistical indicator is normalized by the maximum value among the three

Table 1
Abbreviation and calculation equations of FRA statistical indicators.

Abbreviation	Definition	Equations
ED	Euclidean Distance [10]	$ED = \sqrt{\sum_{i=1}^{N}((Y(i)-X(i))^2}$
SSRE	Sum Squared Ratio Error [1]	$SSRE = \frac{1}{N}\sum_{i=1}^{N}(\frac{Y(i)}{X(i)}-1)^2$
δ	Spectrum deviation [10]	$\delta = \frac{1}{N}\sum_{i=1}^{N}\sqrt{(\frac{X(i)-(Y(i)+X(i))/2}{(Y(i)+X(i))/2})^2+(\frac{Y(i)-(Y(i)+X(i))/2}{(Y(i)+X(i))/2})^2}$
ASLE	Absolute Sum of Logarithmic Error [14]	$ALSE = \frac{\sum_{i=1}^{N}20\log_{10}Y(i)-20\log_{10}X(i)}{N}$
cc	Correlation Coefficient [10]	$cc = \frac{\sum_{i=1}^{N}X(i)Y(i)}{\sqrt{\sum_{i=1}^{N}[X(i)]^2\sum_{i=1}^{N}[Y(i)]^2}}$
ρ	Normalized correlation coefficient [11]	$\rho = \frac{\sum_{i=1}^{N}X^*(i)Y^*(i)}{\sqrt{\sum_{i=1}^{N}[X^*(i)]^2\sum_{i=1}^{N}[Y^*(i)]^2}}$ $X^*(i) = \lvert X(i)\rvert - \frac{1}{N}\sum_{i=1}^{N}X(i)$ $Y^*(i) = \lvert Y(i)\rvert - \frac{1}{N}\sum_{i=1}^{N}Y(i)$
DABS	Absolute difference [14]	$DABS = \frac{\sum_{i=1}^{N}\lvert Y(i)-X(i)\rvert}{N}$
E	Expectation [10]	$E = \frac{1}{N}\sum_{i=1}^{N}\Delta(i)$ $\Delta(i) = \frac{\lvert Y(i)-X(i)\rvert}{\frac{1}{N}\sum_{i=1}^{N}\lvert X(i)\rvert}$
MM	Minimum-Maximum ratio [22]	$MM = \frac{\sum_{i=1}^{N}min(Y(i),X(i))}{\sum_{i=1}^{N}max(Y(i),X(i))}$
SD	Standard Deviation [13,14]	$SD = \sqrt{\frac{\sum_{i=1}^{N}((Y(i)-X(i))^2}{N-1}}$

"$X(i)$" and "$Y(i)$" are the ith amplitude elements of the fingerprint and measured FRA signature, respectively.
N is the number of elements within the frequency range.

Table 2
Examples of feature construction(ED and CC).

Statistical indicators	*ED*			*CC*		
Frequency ranges (kHz)	<100	100–600	>600	<100	100–600	>600
No.1	ED_{1L}	ED_{1M}	ED_{1H}	CC_{1L}	CC_{1M}	CC_{1H}
No.2	ED_{2L}	ED_{2M}	ED_{2H}	CC_{2L}	CC_{2M}	CC_{2H}
…	…	…	…	…	…	…
No.n	ED_{nL}	ED_{nM}	ED_{nH}	CC_{nL}	CC_{nM}	CC_{nH}

sub-frequency bands. The calculation equation is as follows in Equation (5). Most indicators, such as the indicator *ED*, *SD* and *ASLE*, belong to the second type.

$$Z_i = \frac{Y_i}{Y_{LMH}} = \frac{Y_i}{|Y_i|_{max}} \tag{5}$$

where Y_i is the value of a certain statistical indicator in a certain sub-frequency band, Y_{LMH} is the absolute maximum value of this statistical indicator in the three sub-frequency bands, and Z_i is the normalized value.

4. Analysis based on simulation of the lumped parameter equivalent electrical model of transformer winding

Flow Chart of the Electrical Circuit Simulation

The mass FRA signature data of field tests are difficult to collect. Thus, the characteristic of winding deformation can be analyzed by advanced modeling techniques. The finite element method (FEM) is used to simulate transformer winding behaviors in this study. Typical winding deformation faults include radial deformation (RD), axial displacement (AD), inter-disk short circuit (SC) and disk space variation (DSV) fault. A large number of FRA data of these typical winding faults are obtained and analyzed by the spectral clustering algorithm. The flow chart of electrical circuit simulation is shown in Fig. 2.

4.1. FEM and electrical model of the transformer

An 11.55/0.412 kV, 10 kVA transformer is used for simulation, and the dimension parameters of the transformer are shown in Table 3. The windings are designed in rectangular shape, where the HV winding comprises 6 disks with 1134 turns per disk, while the LV winding is a continuous layer of 140 turns. The winding connection type is Dyn1. Fig. 3 shows an image of the actual transformer and the corresponding

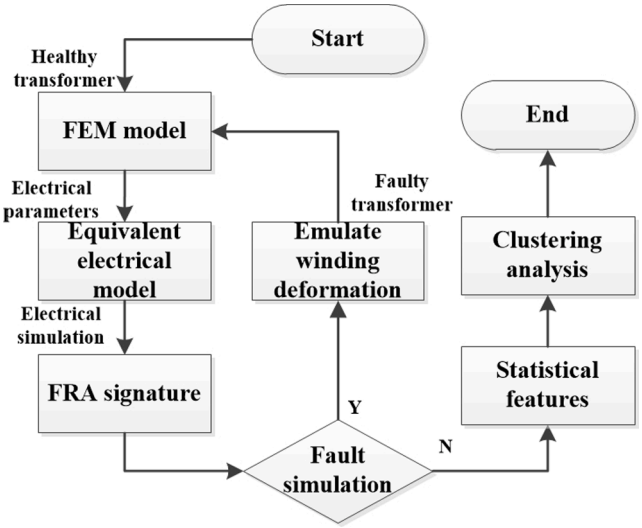

Fig. 2. Flow chart of the electrical circuit simulation.

Table 3
Design specifications of specifically manufactured transformer.

Location	Parameter	Value/mm
HV winding	Length of external diameter	200
	Width of external diameter	162
	Length of internal diameter	168
	Width of internal diameter	130
	Height	468
LV winding	Length of external diameter	108
	Width of external diameter	108
	Length of internal diameter	100
	Height	468
Core	Length of core section	92
	Width of core section	92
	Length of core	710
	Height of core	680

FEM model.

The equivalent electrical parameters of the transformer in healthy status are calculated by FEM simulation. The lumped parameter electrical circuit is presented in Fig. 4. The definition of each parameter can be found in [4]. The electrical parameters of equivalent model are shown in Table 4.

4.2. Simulated FRA signatures of various winding faults

The winding RD is simulated by FEM on the HV winding, the winding free buckling with different fault degrees are emulated on HV5 disk (seen from top to bottom), and the fault degree is defined by the ratio of the radial deformed part to the diameter of winding. Fig. 5 shows some deformed windings.

The variable winding RD faults are simulated, the fault degree varies from 1.2% to 37%, and there are 30 groups of faults. The FEM simulation results reveal that the winding RD mainly induces variations in the parameter C_{gh} and L_{sh} of the HV winding, which corresponds to the deformed disk; further, the variation in C_{hl} between the deformed HV winding and the LV winding is also significant.

In addition, the winding AD fault is also simulated by the FEM method, and this fault is emulated on HV1 ~ HV6 windings. The fault degree is defined as the ratio of the AD offset to the height of HV winding. Fig. 6 shows some typical deformed windings.

The variable winding AD faults are simulated by a parameter sweep, the fault degree varies from 0.04% to 4%, the interval of the fault degrees is set to be equal, and there are 90 groups of faults. The FEM simulation results show that this type of fault mainly induces variations in C_{hl} and K_{hl} between the HV winding and the corresponding LV winding. Impacts of winding RD and AD faults on equivalent electrical parameters are shown in Fig. 7.

According to the calculated electrical parameters, the FRA signatures of faulty winding with different fault types, degrees and locations can be simulated based on the electrical circuit. The faults are set in the top (HV1 disk), middle (HV3 disk) and bottom (HV6 disk) of transformer HV winding to simulate different fault locations. The end to end open circuit FRA signatures of faulty winding are obtained.

First, the winding RD faults are simulated. In each fault location, there are 30 groups of different fault degrees. The total number of RD groups is 90. Second, the winding AD faults are simulated on HV winding, and a total of 90 groups of FRA are obtained. In addition, the winding inter-disk SC fault is simulated by shortening two basic units of the electrical model with a variable resistance, to simulate insulation failures with different fault degrees. There are 30 groups of inter-disk SC faults on the top, middle and bottom of the HV winding, respectively. Moreover, the winding DSV fault is simulated in this study. As described in [13], a capacitor with variable capacitance is paralleled with two basic units of electrical model to simulate the DSV fault, with different fault degrees and locations. There are 30 groups of DSV faults on the top, middle and bottom, respectively. Due to space limitation of the paper,

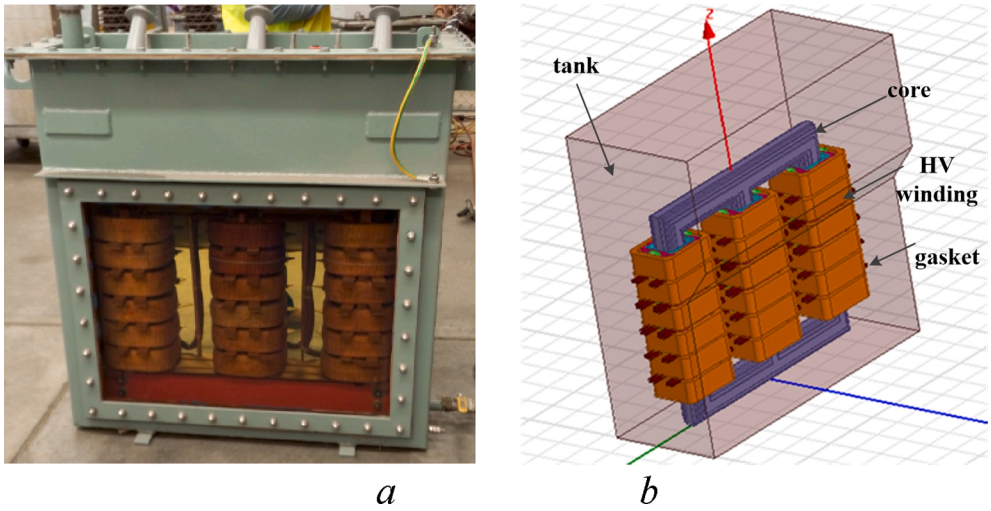

Fig. 3. Image of actual transformer and corresponding FEM model. (a) image of actual transformer, (b) FEM model.

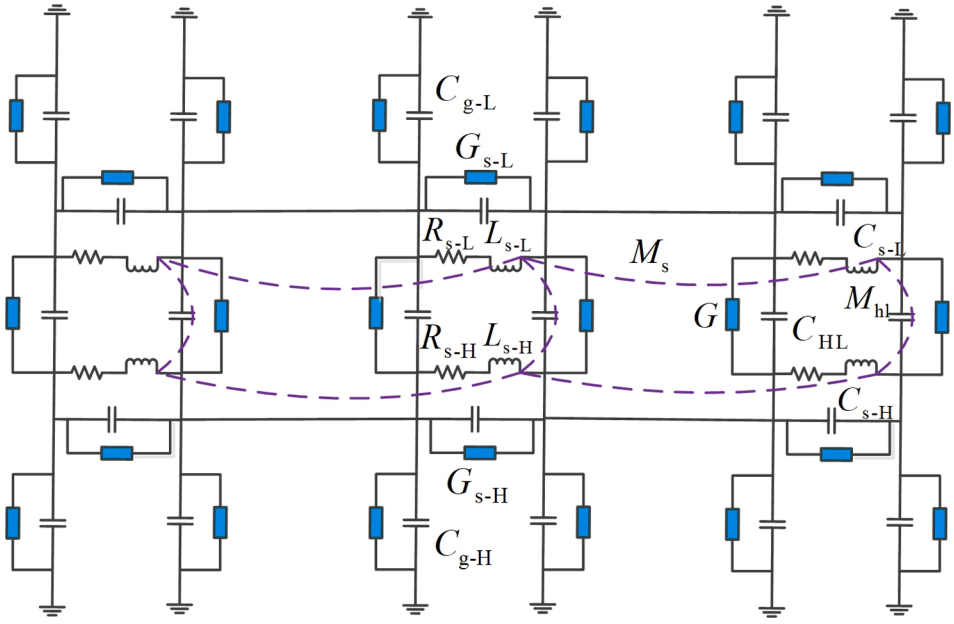

Fig. 4. Equivalent lumped parameter electrical circuit of the transformer.

Table 4
Equivalent electrical parameters of model transformer winding.

	C_g	C_s	C_{HL}	L_s	K_{HL}	K_{ij}
HV winding	9 pF	45.2 pF	58.2 pF	254.7 mH	0.513	0.327
LV winding	49.7 pF	10.3 pF	58.2 pF	1.79 mH	0.513	0.219

partial fault FRA signatures are shown in Fig. 8. It is noted that the oscillations in the frequency range below about 0.05 MHz are also the part of FRA resonances and anti-resonances.

4.3. Clustering analysis of the simulated FRA signatures

A total of 360 groups of FRA data with four fault types are obtained, as described in section III, the statistical features are calculated and standardized, and input to the spectral clustering algorithm. The feature data are a 360*30 matrix. 30 are the numbers of features, which is calculated from 10 statistical indices in three sub-frequency bands. The MATLAB visualization tool t-SNE (t-Distributed Stochastic Neighbor Embedding, t-SNE) is used to visualize the high dimensional data. A visualization of the clustering result of input statistical features without fault type information is shown in Fig. 9. By contrast, the distribution of original labels for four fault types is shown in Fig. 10. The following analysis can be derived:

1) The clustering result of the simulated FRA features by the spectral clustering algorithm is consistent with the distribution of the original labels of FRA features, which demonstrates the feasibility of spectral clustering algorithm on processing transformer FRA data.

2) By comparing Fig. 9 with Fig. 10, the clustering result of "1″ is the SC fault, the clustering result of "2" is the AD fault, the clustering result of "3" is the DSV fault, and the clustering result of "4" is the RD fault. Different winding fault types fall into different clusters, which indicate the separability of four winding deformation fault types.

3) There are three specific branches for both DSV and RD faults, which correspond to the location setup of faults, namely, the top, middle and bottom of HV windings. Moreover, in each branch, the distribution of faulty FRA data can be observed, which corresponds to the degree setup of two faults.

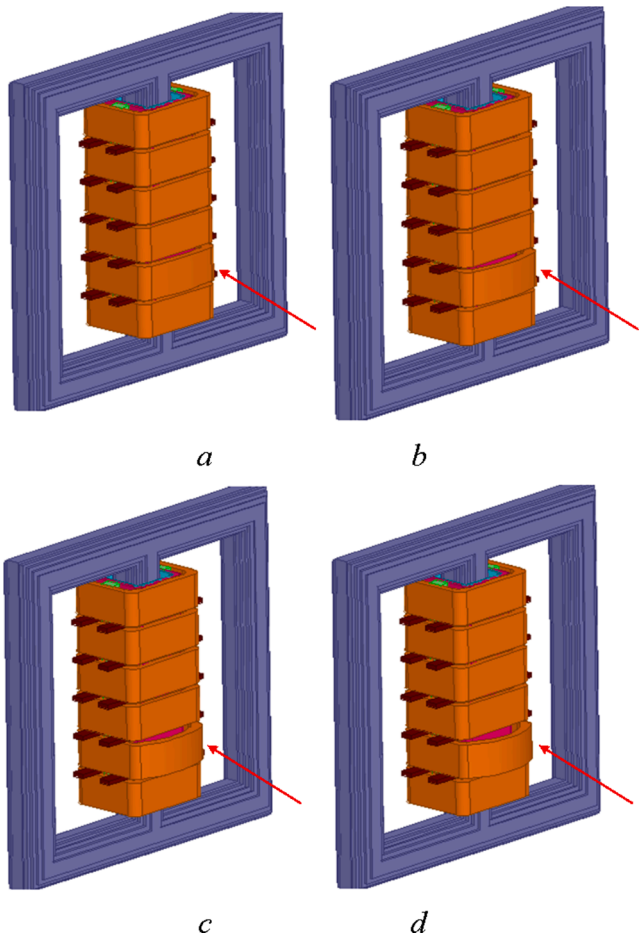

Fig. 5. Some radially deformed winding models with different fault degrees. (a) 5%, (b) 9.3%, (c) 15.4%, (d) 21.6%.

4) In AD fault simulation, all faults are produced on the HV winding and arranged in the axial direction, and no fault location setup is applied. Thus, there is only one branch for the winding AD fault clustering result. In addition, the distribution of AD clustering result is similar to those of DSV and RD faults, due to the successive fault degree setup.

5) In the clustering result of the SC fault, three clusters can be observed, which correspond to the location setup of this fault. Within each cluster, the fault data show an "annulus" distribution.

6) It can be concluded that the fault degree of the winding DSV, AD and RD faults can be distinguished based on the clustering analysis, which shows the separability of these fault degrees. Whereas it is difficult to recognize the degree of the winding SC faults, which might be due to the impact of this fault on electrical parameters is not linear.

7) Besides, the fault locations are setup in the top, middle and bottom of HV winding in equivalent electrical circuit of Fig. 4, the locations of the winding DSV, RD and SC faults are separable based on the phenomenon that each fault location shows a specific branch or cluster. However, it should be further discussed and verified for the situation that the fault is set between the two locations mentioned above.

5. Evaluation of clustering result validity

5.1. Evaluation index of clustering quality

The evaluation indexes of clustering quality can be divided into external and internal indexes. In the external index, the clustering algorithm is used to process datasets with clear category labels, and these indexes are then used to calculate the accuracy of the clustering result. The internal indexes are the predefined evaluation criteria, which are normally used to describe the inherent characteristics of the obtained clusters.

The common external evaluation indexes include RI (Rand index), ARI (adjust Rand index) and FMI (Fowlkes-Mallows index). Besides, in this study, the DBI (Davies-Bouldin index) is selected as the internal evaluation index. The definitions of these indexes can be found in [23].

The RI, which varies from 0 to 1, calculates the similarity between the clustering result and the actual labels. The larger the RI is, the more consistent the clustering result is with the actual situation. The value of the ARI also varies from 0 to 1, and the closer the value is to 1, the more satisfactory the quality of the clustering result is. The FMI is defined as the geometric mean of the pairwise precision and the recall, and the value is 0–1. Larger FMI indicator values indicate that the obtained clusters are closer to the standard clusters. The DBI is defined as the sum of the average distance between the samples of two clusters C_i and C_j divided by the distance between the center points μ of the two clusters. The smaller the DBI value is, the better the performance of the clustering result is.

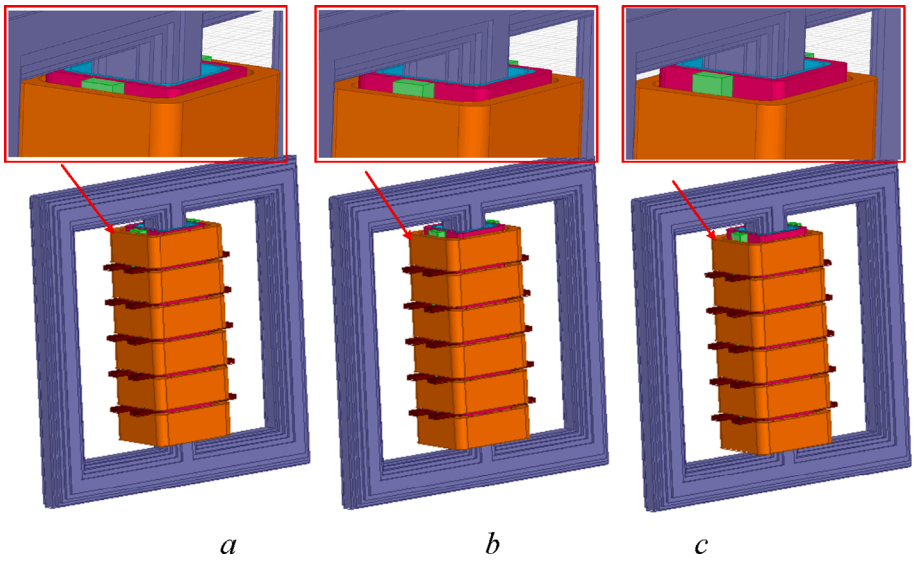

Fig. 6. Some winding models of AD with different fault degrees. (a) 1.1%, (b) 2.2%, (c) 3.3%.

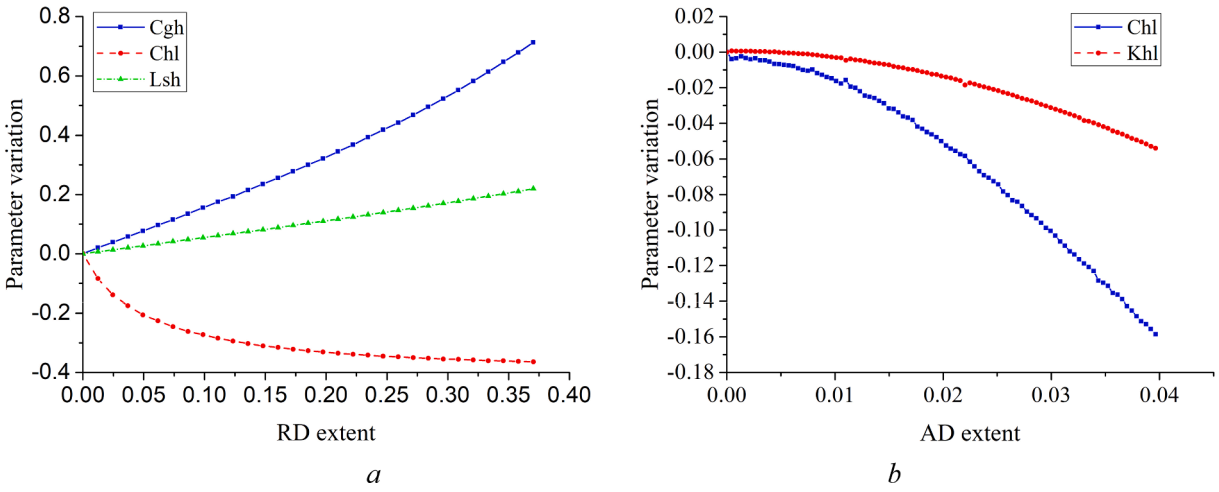

Fig. 7. Impacts of winding RD and AD faults on equivalent electrical parameters. (a) RD fault, (b) AD fault.

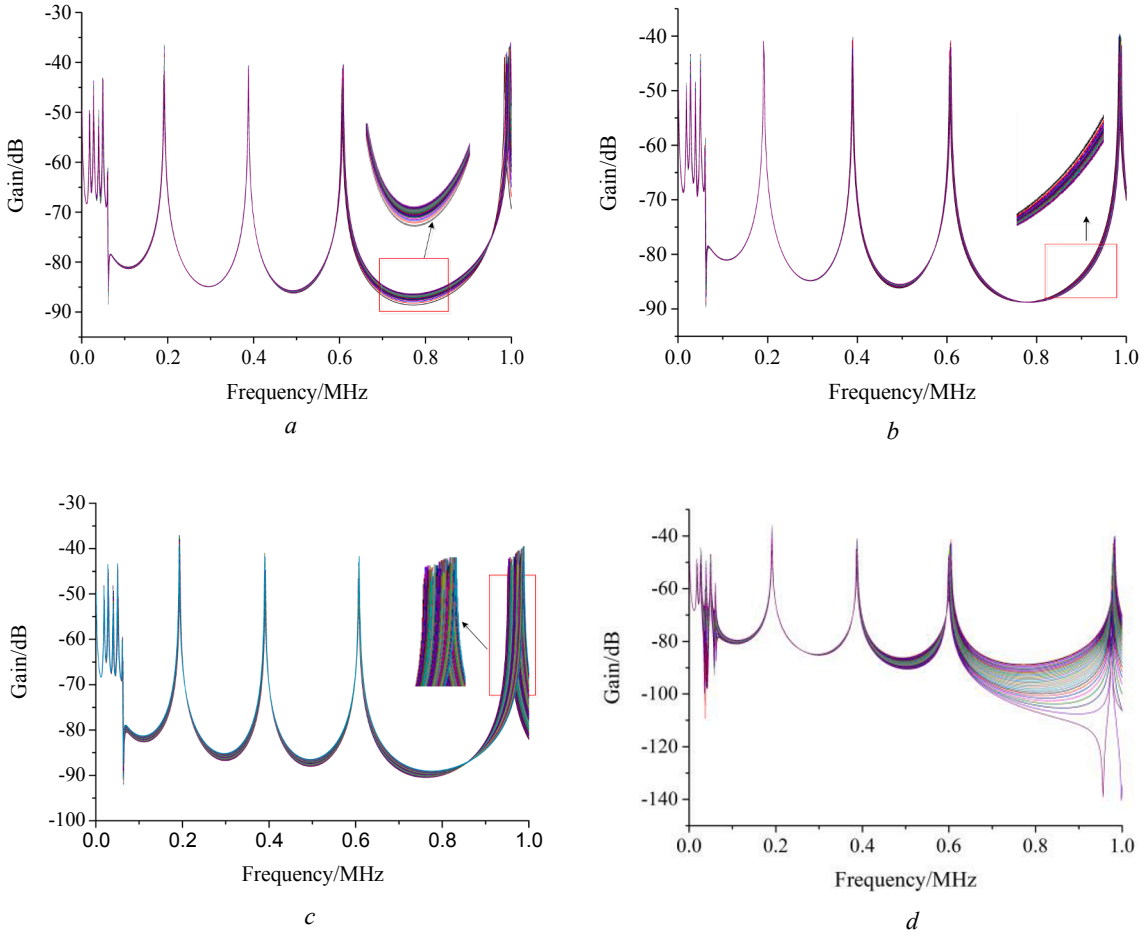

Fig. 8. Typical fault FRA signatures of HV phase-A winding based on FEM simulation. (a) RD faults on the top, (b) RD faults on the middle, (c) AD faults, (d) DSV faults on the top.

5.2. Robustness and global optimization ability index of the clustering algorithm

Suppose a specific evaluation index F, which can be an external or internal indicator, is selected. The same data are tested m times by the same clustering algorithm. The global optimization ability of the clustering algorithm determines if the clustering results are stable at a high level, according to the following equation:

$$F_{\text{mean}} = \frac{1}{m}\sum_{i=1}^{m} F_i \tag{6}$$

where F_i is the evaluation index of the ith clustering test, and F_{mean} is the mean value.

The robustness of the clustering algorithm can be defined as the

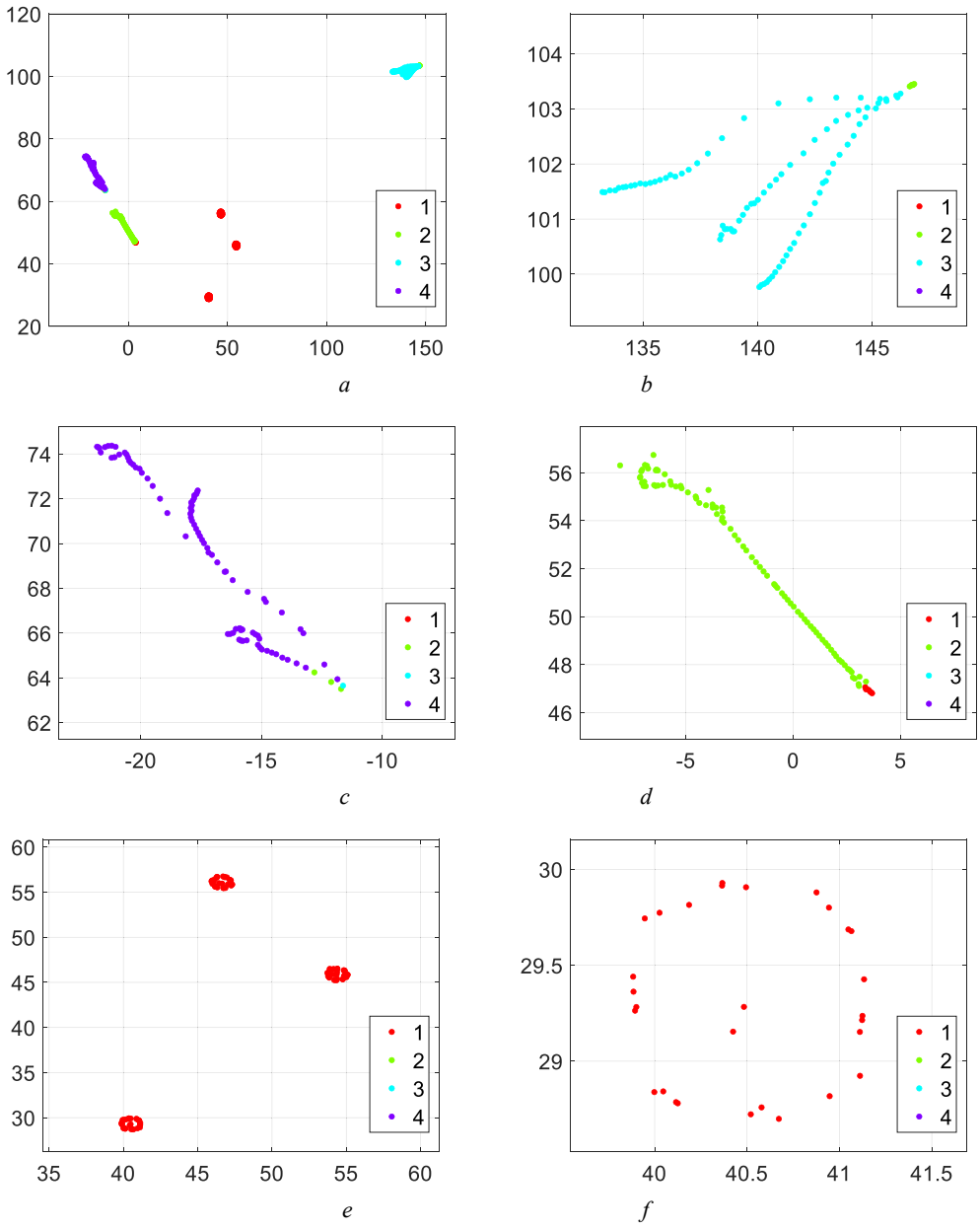

Fig. 9. Clustering result without fault type information. (a) Overall image, (b) local enlarged image with the clustering result of 3, (c) local enlarged image with the clustering result of 4, (d) local enlarged image with the clustering result of 2, (e) local enlarged image with the clustering result of 1, (f) local enlarged image with the clustering result of 3 in the same location.

similarity degree of the clustering results, in which the same data are processed by the same algorithm several times. The robustness index is as follows:

$$F_{\mathrm{va}} = \sum_{i=1}^{m} \left\| F_i - F_{\mathrm{mean}} \right\|^2 \tag{7}$$

where F_{va} is the variance of the clustering results for m times.

In general, the larger the F_{mean} is and the smaller the F_{VA} is, the better the global optimization ability and robustness of the clustering algorithm are.

5.3. Comparison with other conventional clustering algorithms

To verify the applicability of spectral clustering method on processing FRA data, other common clustering algorithms, including the K-means, FCM (Fuzzy C-Means), hierarchical clustering and Gauss clustering, are also used to process the transformer simulated FRA data. The proposed external and internal indexes are used to evaluate the clustering result of each algorithm. To avoid the occasionality, these algorithms are repeatedly tested several times, and the best results are chosen and shown in Table 5. It can be seen that the RI, ARI, FMI and DBI values of the spectral clustering method are larger than those of the other clustering algorithms.

To compare the global optimization ability and robustness of these clustering algorithms, all algorithms are repeatedly tested 20 times, and the RI indicator is used for evaluation. The results are shown in Fig. 11. It can be concluded that the clustering result of the spectral clustering algorithm has a much higher quality, which converges to the global optimal solution with a larger probability.

In addition, the global optimization ability and robustness index of Fig. 11 are calculated and are shown in Table 6. It can be derived that the F_{mean} index of the spectral clustering algorithm is the largest among all

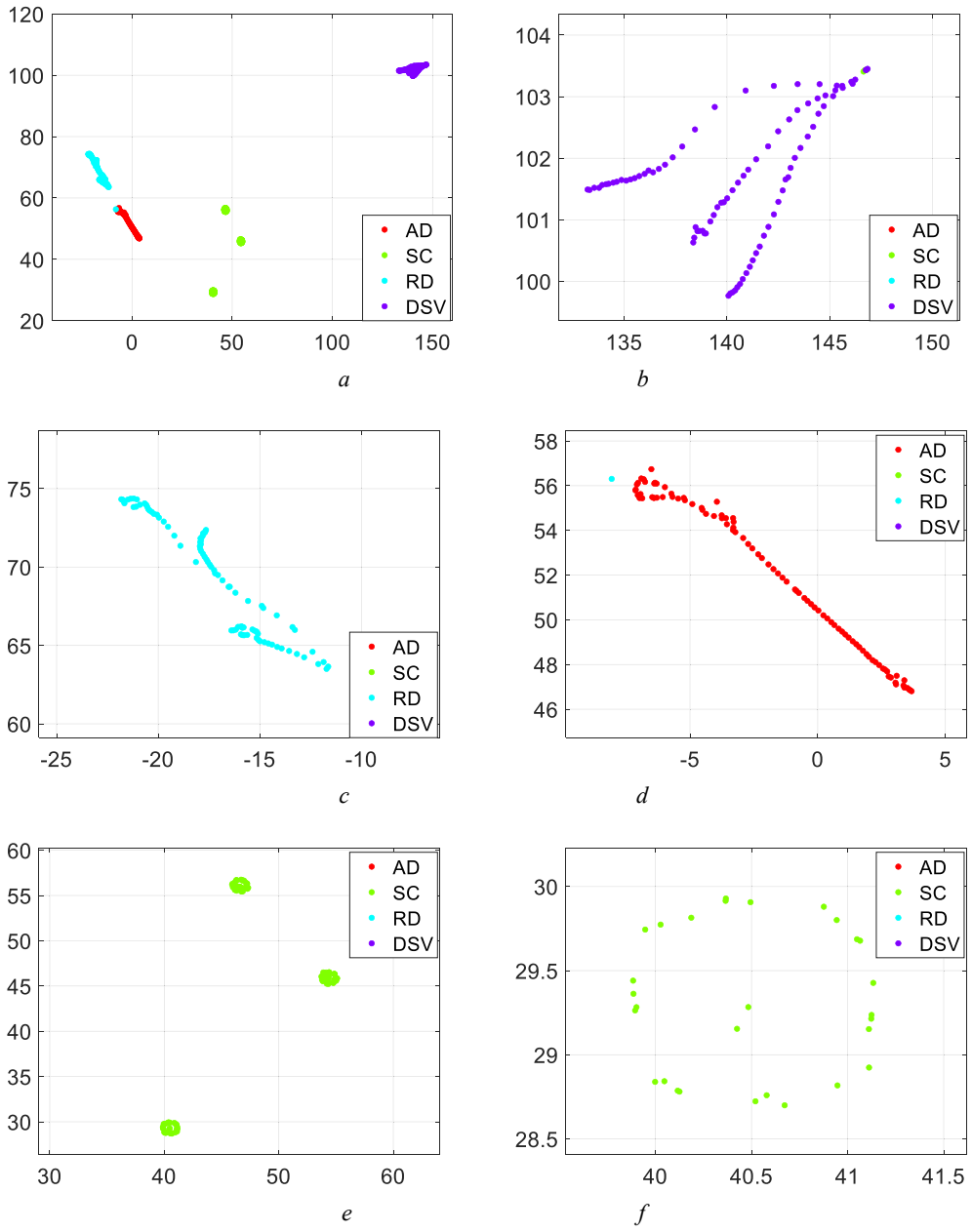

Fig. 10. Distribution of original labels for four fault types. (a) Overall image, (b) local enlarged image of DSV faults, (c) local enlarged image of RD faults, (d) local enlarged image of AD faults, (e) local enlarged image of SC faults, (f) local enlarged image of SC faults in the same location.

Table 5
Evaluation indexes of clustering results by different clustering algorithms.

Algorithms	*RI*	*ARI*	*FMI*	*DBI*
K-means	0.8964	0.7242	0.7934	0.7170
FCM	0.8834	0.6899	0.7678	0.7510
Hierarchical	0.7878	0.4683	0.6153	0.6018
Gauss	0.8556	0.6179	0.7146	0.8885
Spectral clustering	0.9484	0.8617	0.8960	0.8948

the clustering algorithms. The F_{va} index of the spectral clustering algorithm is the second smallest. The F_{va} index of the hierarchical clustering algorithm is 0, and its robustness is best. However, the global optimization ability of hierarchical clustering is not as good as that of the spectral clustering algorithm.

6. Experimental verification of a model transformer

6.1. FRA signatures of emulated faulty winding

Groups of emulated winding deformation experiments are performed on a test platform in previous study [13]. The tested transformer is a specially manufactured core-type model transformer with a voltage ratio of 10/0.4 kV and the capacity of 400 kVA, as shown in Fig. 12. A total of 45 groups of faulty windings are emulated, including 15 groups of RD faults, 15 groups of SC faults and 15 groups of DSV faults. In each fault type, different fault degrees and locations are emulated, and FRA curves are obtained. More detailed information about the model transformer and experimental setup can be found in [13]. The results of winding emulated fault are shown in Fig. 13. In Fig. 13, the solid line is healthy FRA signature, while the dotted lines are faulty FRA signatures with different fault status. Specifically, in Fig. 13(a), the defined term "1–2" means that there is an inter-disk SC fault between 1# disk and 2#

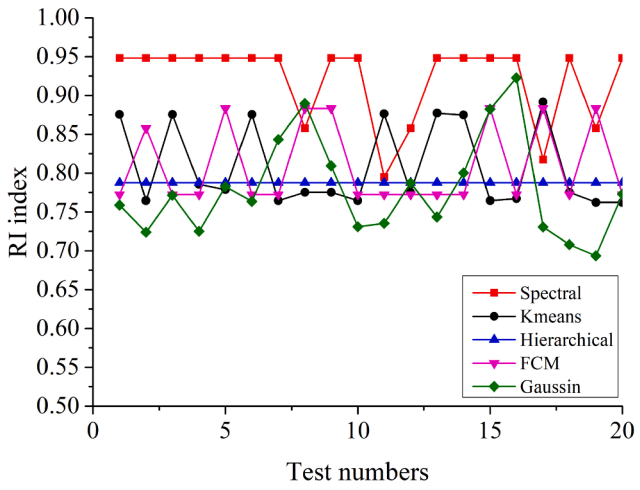

Fig. 11. RI indicators of the clustering result after processing with the spectral, K-means, FCM, hierarchical and Gauss clustering algorithms for 20 times.

Table 6
Global optimization ability and robustness index of different clustering algorithms.

Algorithms	F_{mean}	F_{va}
K-means	0.8081	0.0537
FCM	0.8099	0.0531
Hierarchical	0.7878	0
Gauss	0.7788	0.0760
Spectral clustering	0.9205	0.0497

disk. For Fig. 13(b), for instance, in the defined term "5–5%-4", the first number "5" means 5 disks are radially deformed; the second number "5%" indicates the RD fault degree, the third number "4" means that the deformations are produced in four directions of winding disk. For Fig. 13 (c), for instance, in the defined term "34-50p", the first number "34" means that the DSV fault is produced between 3# disk and 4# disk, while the second term "50p" indicates the paralleled capacitance.

6.2. Clustering analysis

In order to verify the conclusions of simulation from the perspective of experiment, the proposed procedure is applied to process the above small amount of experimental FRA data. The statistical features are extracted, normalized, and imported into the spectral clustering algorithm. The input feature is a 45*30 matrix. The clustering result and the distribution of the original FRA data with labels are shown in Fig. 14.

Compare Fig. 14(a) and (b), the distribution of the FRA data after clustering is consistent with the original labels. There are boundaries between the winding RD, SC and DSV faults, except for two points, which could be caused by the similarity of two FRA signatures for DSV and RD fault. In each fault type, the FRA data are clustered. Further, because the fault degree is not consistently established in the setup of RD fault, the distribution of RD fault presents the characteristics of the cluster shape. While in DSV cluster, there is the characteristic of a local branch distribution because the fault degree setup is approximately continuous in each fault location. The above analysis indicates that the conclusions obtained from experimental data are similar to those of simulation study in part D, section IV. The spectral clustering algorithm is suitable for processing FRA data, and the winding main deformation fault types are separable. In addition, the evaluation indexes of the clustering quality are calculated and shown in Table 7. Fig. 14 and Table 7 indicate the effectiveness and superiority of the spectral clustering algorithm.

7. Conclusion

For the first time, the spectral clustering of transformer FRA signatures is studied. A procedure of clustering is introduced. Several statistical indicators of FRA signatures are calculated and extracted as the input features. A total of 360 groups of FRA signatures under RD, AD, SC and DSV faults with different fault degrees and locations are obtained on a verified transformer model based on FEM simulation. The spectral clustering algorithm is used to process these signatures and to analyze the FRA characteristics. Other common clustering algorithms are also applied and compared. Moreover, some indexes are introduced to evaluate the accuracy, robustness and global optimization ability of the clustering algorithms. Finally, the experimental FRA signatures, obtained from the artificial fault simulation of a 10 kV model transformer, are used to verify the electrical simulation and analysis. The following conclusions can be derived:

- The clustering result of the simulated FRA data processed by the spectral clustering algorithm is almost consistent with the distribution of the original FRA labels, which indicates the applicability of the spectral clustering algorithm for processing FRA data.
- The evaluation of the clustering accuracy, robustness and global optimization ability indicates the superiority of the spectral clustering algorithm for processing FRA data, compared to those of other common clustering algorithms.

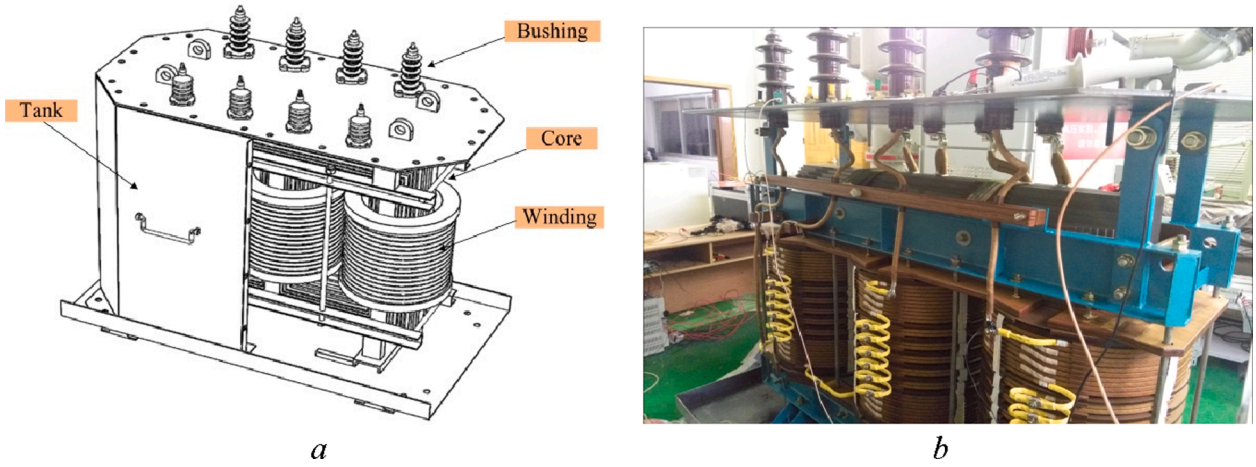

Fig. 12. Tested model transformer with its tank uncovered. (a) Internal configuration of model transformer. (b) An image of model transformer.

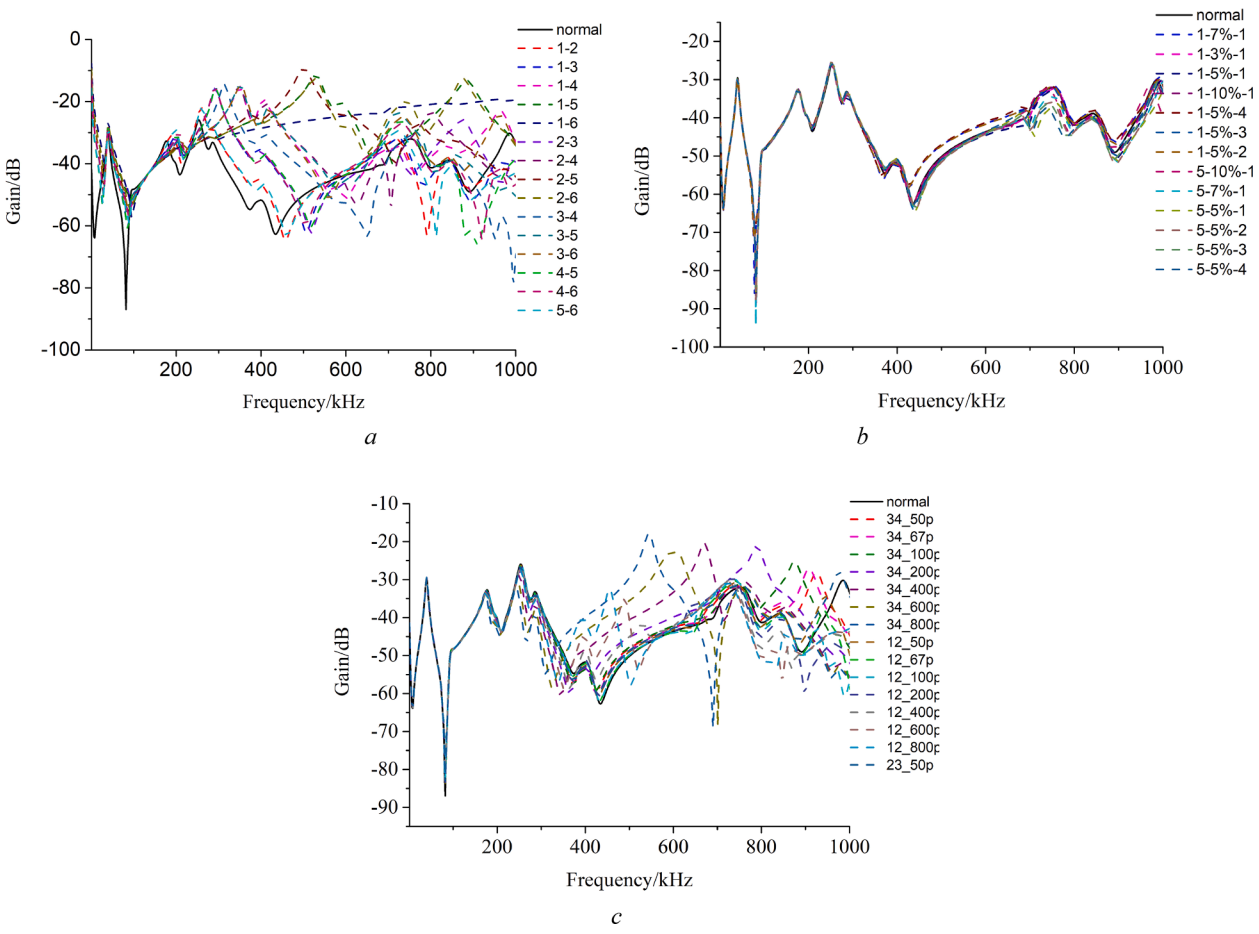

Fig. 13. Measured FRA signatures of model transformer. (a) Simulated inter-disk SC fault. (b) Simulated RD fault. (c) Simulated DSV fault.

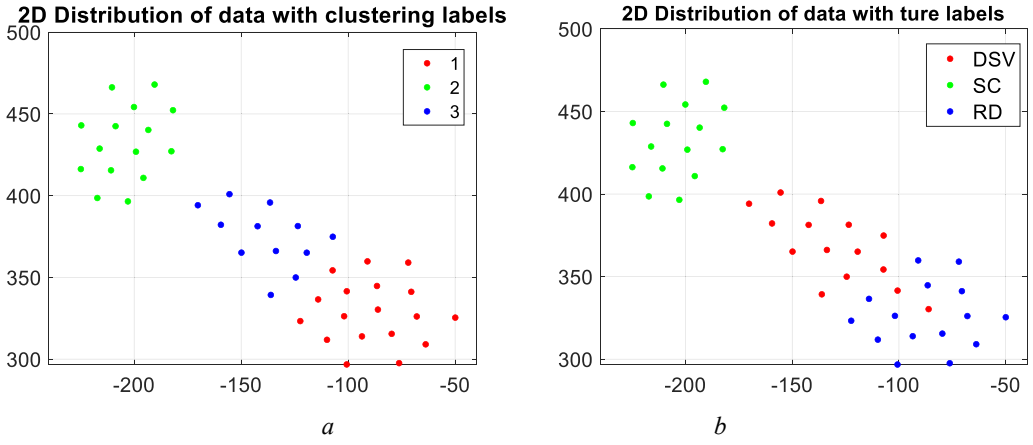

Fig. 14. Distribution of the clustering result and original FRA statistical features. (a) clustering results without fault type information, (b) original distribution of FRA statistical features with RD, SC and DSV faults.

Table 7
Evaluation indexes of clustering results by different clustering algorithms.

Algorithms	*RI*	*ARI*	*FMI*	*DBI*
K-means	0.6113	0.8222	0.7496	0.6324
FCM	0.4058	0.7101	0.6422	0.6675
Hierarchical	0.4326	0.7182	0.6671	0.6889
Gauss	0.4911	0.7768	0.6564	1.5888
Spectral clustering	0.9182	0.8129	0.8733	0.8244

- Different winding fault types fall into different clusters, and there are obvious boundaries between them, which indicate the separability of four winding deformation fault types.
- The winding DSV, AD and RD fault present branch distribution characteristic in clustering result, and the degrees of these faults may be separable. Whereas in the SC fault clustering results, clusters can be observed, and the fault data show an “annulus” distribution. It is not easy to recognize the fault degree in winding SC faults, which

might be due to the impact of this fault on electrical parameters is not linear.

- The locations of the winding DSV, RD and SC faults are separable based on the phenomenon that each fault location shows a specific branch or cluster, which corresponds to the fault setup in the top, middle and bottom of HV winding.

The characteristic of winding deformation faults implies that main winding faults can be identified and classified when some advanced machine learning algorithms are used, which are the state-of-the-art AI algorithms exactly study. In addition, the FEM simulation was verified on an oil-immersed transformer. However, the data analytic result has not been valid for a dry type transformer at present, which will be studied in the future.

Declaration of Competing Interest

The author declare that there is no conflict of interest.

Acknowledgments

This work was supported in part by the National Natural Science Foundation of China under Grant 51807166 and in part by the Natural Science Foundation of Chongqing under Grant cstc2019jcyj-msxmX0236.

Data availability

The raw/processed data required to reproduce these findings cannot be shared at this time as the data also forms part of an ongoing study.

References

[1] Tarimoradi H, Gharehpetian GB. Novel calculation method of indices to improve classification of transformer winding fault type, location, and extent. IEEE Trans Ind Info 2017;13(4):1531–40.
[2] Bagheri M, Zollanvari A, Nezhivenko S. Transformer fault condition prognosis using vibration signals over cloud environment. IEEE Access, 6, 2018, pp. 9862–9874.
[3] Portilla WH, Mayor GA, Guerra JP, Garcia CG. Detection of transformer faults using frequency-response traces in the low-frequency bandwidth. IEEE Trans Ind Electron 2014;61(9):4971–8.
[4] Hashemnia N, Abu-Siada A, Islam S. Improved power transformer winding fault detection using fra diagnostics – part 2: radial deformation simulation. IEEE Trans Dielectr Electr Insul 2015;22(1):564–70.
[5] García B, Burgos JC, Alonso AM. Winding deformations detection in power transformers by tank vibrations monitoring. Electr Power Syst Res 2005;74(1):129–38.
[6] Mortazavian S, Shabestary MM, Mohamed YA, Gharehpetian GB. Experimental studies on monitoring and metering of radial deformations on transformer HV winding using image processing and UWB transceivers. IEEE Trans Ind Info 2015;11(6):1334–45.
[7] Arri E, Carta A, Mocci F, Tosi M. Diagnosis of the state of power transformer windings by on-line measurement of stray reactance. IEEE Trans Instrum Meas 1993;42(2):372–8.
[8] Cheng Q, Zhao ZY, Tang C, Qian GC, Islam S. Diagnostic of transformer winding deformation fault types using continuous wavelet transform of pulse response. Measurement 2019;2019(140):197–206.
[9] Siada AA, Islam S. A novel online technique to detect power transformer winding faults. IEEE Trans Power Del 2012;27(2):849–57.
[10] Senobari RK, Sadeh J, Borsi H. Frequency response analysis (FRA) of transformers as a tool for fault detection and location: a review. Electr Pow Syst Res. 2018;155:172–83.
[11] Frequency response analysis on winding deformation of power transformers, People Republic of China, Electric Power Industry Standard, DL/T911-2004, ICS27.100, F24, Document No. 15182-2005, 2005 (in Chinese).
[12] Measurement of Frequency Response, IEC Standard 60076-18, Ed. 1.0, 2012-07.
[13] Zhao ZY, Yao CG, Li CX, Islam S. Detection of power transformer winding deformation using improved FRA based on binary morphology and extreme point variation. IEEE Trans Ind Electron 2018;65(4):3509–19.
[14] Rahimpour E, Christian J, Feser K, Mohseni H. Transfer function method to diagnose axial displacement and radial deformation of transformer windings. IEEE Trans Power Del 2003;18(2):493–505.
[15] Samimi MH, Tenbohlen S, Akmal AAS, Mohseni H. Evaluation of numerical indices for the assessment of transformer frequency response. IET Gener Transm Dis 2017;11(1):218–27.
[16] Samimi MH, Tenbohlen S, Akmal AAS, Mohseni H. Improving the numerical indices proposed for the FRA interpretation by including the phase response. Int J Electr Power Energy Syst 2016;83:585–93.
[17] Zhang ZW, Tang WH, Ji TY, Wu QH. Finite-element modeling for analysis of radial deformations within transformer windings. IEEE Trans Power Del 2014;29(5):2297–305.
[18] Shah KR, Ragavan K. Assessing mechanical deformations in two-winding transformer unit using reduced-order circuit model. Int J Electr Power Energy Syst 2016;79:235–44.
[19] Bagheri S, Gharehpetian GB. Classification and discrimination among winding mechanical defects, internal and external electrical faults, and inrush current of transformer. IEEE Trans Ind Info 2018;14(2):484–93.
[20] Bigdeli M, Vakilian M, Rahimpour E. Transformer winding faults classification based on transfer function analysis by support vector machine. IET Electr Power App 2012;6(5):268–76.
[21] Liu JN, Zhao ZY, Tang C, Yao CG, Li CX, Islam S. Classifying transformer winding deformation fault types and degrees using FRA based on support vector machine. IEEE Access 7;2019:112494–112504.
[22] Gonzales JC, Mombello EE. Fault interpretation algorithm using frequency-response analysis of power transformers. IEEE Trans Power Del 2016;31(3):1034–42.
[23] Luxburg UV. A tutorial on spectral clustering. Stat comput 17(4);2007:395–416.
[24] Xiong YR, Zhang RQ, Zhang FY, Yang WY, Kang QD, Chen WC, et al. A spectra partition algorithm based on spectral clustering for interval variable selection. Infrared Phys Technol 2020;105:1–9.
[25] Nardo AD, Natale MD, Giudicianni C, Greco R, Santonastaso GF. Weighted spectral clustering for water distribution network partitioning. Appl Network Sci 2017;105:2–19.
[26] Samimi MH, Tenbohlen S. FRA interpretation using numerical indices: State-of-the-art. Int J Electr Power Energy Syst 2017;89:115–25.
[27] Rahimpour E, Jabbari M, Tenbohlen S. Mathematical comparison methods to assess transfer functions of transformers to detect different types of mechanical faults. IEEE Trans Power Del 2010;25(4):2544–55.